Dissociative ionization of neon clusters Ne[sub n], n=3 to 14: A realistic multisurface dynamical study

David Bonhommeau, Alexandra Viel, Nadine Halberstadt

Dissociative ionization of neon clusters Ne_n, $n=3$ to 14: A realistic multisurface dynamical study

David Bonhommeau, Alexandra Viel,[a] and Nadine Halberstadt[b]
Laboratoire de Physique Quantique, IRSAMC, UMR 5626, CNRS et Université P. Sabatier, 118 Route de Narbonne, F-31062—Toulouse, France

(Received 24 March 2005; accepted 23 May 2005; published online 9 August 2005)

The molecular dynamics with quantum transitions (MDQT) method is applied to study the fragmentation dynamics of neon clusters following vertical ionization of neutral clusters with 3 to 14 atoms. The motion of the neon atoms is treated classically, while transitions between the adiabatic electronic states of the ionic clusters are treated quantum mechanically. The potential energy surfaces are described by the diatomics-in-molecules model in a minimal basis set consisting of the effective $2p$ orbitals on each neon atom for the missing electron. The fragmentation mechanism is found to be rather explosive, with a large number of events where several atoms simultaneously dissociate. This is in contrast with evaporative atom by atom fragmentation. The dynamics are highly nonadiabatic, especially at shorter times and for the larger clusters. Initial excitation of the neutral clusters does not affect the fragmentation pattern. The influence of spin-orbit coupling is also examined and found to be small, except for the smaller size systems for which the proportion of the Ne^+ fragment is increased up to 43%. From the methodological point of view, most of the usual momentum adjustment methods at hopping events are shown to induce nonconservation of the total nuclear angular momentum because of the nonzero electronic to rotation coupling in these systems. A new method for separating out this coupling and enforcing the conservation of the total nuclear momentum is proposed. It is applied here to the MDQT method of Tully but it is very general and can be applied to other surface hopping methods.
 [DOI: 10.1063/1.1953530]

I. INTRODUCTION

One of the most challenging problems in molecular physics is the study of vibrational and electronic energy transfers at the molecular level (predissociation and intramolecular vibrational relaxation in isolated molecules, caging in solvated molecules, etc.). The study of the size dependence of these processes can provide valuable information on the same processes in the condensed phase. In this context, ideal model systems are provided by van der Waals clusters built with a varying number of rare gas atoms: complexity can be gradually added by increasing the number of rare gas atoms.

Isolated rare gas clusters are known for fragmenting upon ionization.[1–3] This is due to the large difference between equilibrium geometries in the neutral and ionized states. In order to get a complete picture of this process, the ideal experiment would consist in getting the fragmentation pattern for the ionization of a neutral cluster of a given size. Unfortunately, mass selection is easy for ions but not for neutrals. To date the only published experiment in which the neutrals were size-selected prior to ionization (apart from helium clusters) was conducted by Buck and co-workers[3–5] on argon clusters. Size selection of the neutrals was performed by diffraction with helium atoms, and the fragments resulting from the ionization process were detected by mass spectrometry. It was found that fragmentation is indeed very important with a strong preference for the dimer Ar_2^+ channel. Although the equilibrium structure calculations[6,7] indicate that the core ion in these clusters is at least a trimer, Ar_3^+ is only detected for neutral clusters of five or more atoms.

The ionization of rare gas clusters has gained renewed interest more recently as a model to study the friction exerted on moving molecular systems inside superfluid helium nanodroplets.[8–11] Comparing the fragmentation pattern following ionization in the gas phase or inside helium nanodroplets can give information on the influence of the helium environment on the dissociation dynamics, and therefore on the existence of a friction.

We have chosen to study first the dissociation dynamics of ionized neon clusters, because spin-orbit effects are expected to be weak for this member of the rare gas series, while quantum effects associated with the motion of the neon atoms should remain reasonably small. So far no experiment has included size selection of the neutral neon clusters prior to ionization in the analysis of their fragmentation pattern. However, these clusters exhibit very interesting properties. Märk and Scheier[12] have detected special stability ("magic numbers") for $n=14$, 21, 56 and 75, for neon clusters ionized by electron bombardment, whereas the other rare gases (Ar, Kr, Xe) exhibit a well-known special stability for icosahedral structures ($n=13$ and 55). Mass spectra also showed significant drops in intensity ("secondary magic numbers") for $n>9$ and $n>18$. These results were confirmed by Fieber

[a]Present address: PALMS—SIMPA, UMR 6627 du CNRS, Université de Rennes 1, Campus de Beaulieu, F-35042 Rennes, France.
[b]Electronic mail: nadine.halberstadt@irsamc.ups-tlse.fr

et al.[13] in photoionization experiments. In a recent experiment, Gluch *et al.*[14] have studied the microsecond time scale decay of mass selected rare gas ions ($Rg \equiv Ne, Ar, Kr$) and measured the corresponding kinetic energy release, which they used to determine the binding energies of Rg_n^+ ($n \geqslant 10$) by applying finite heat bath theory.[15] Smaller cluster sizes have not been included in their analysis because the statistical model fails below $n=10$. In addition, a ^{22}Ne isotope enrichment effect has been shown by Fieber *et al.*[13] and by Scheier and Märk.[16] This has been attributed by Johnson and co-workers[17] to the ion-molecule exchange reaction $^{22}Ne + {}^{20}Ne_2^+ \rightarrow {}^{20}Ne + {}^{20}Ne^{22}Ne^+$.

From the theoretical point of view, the first studies have concentrated on the determination of the electronic and geometrical equilibrium structure of the neon clusters, in order to interpret the experimental "magic numbers". The first calculation[18] on Ne_3^+ reported a linear symmetric structure. This has been confirmed by more recent high level *ab initio* calculations, which have also proved the accuracy of the diatomics-in-molecules (DIM) model for these clusters.[19] The structure of Ne_n^+ clusters for $n \geqslant 3$ was first studied by Fieber *et al.*[20] using the DIM method.[21] The most recent and accurate results have been obtained by Naumkin and Wales[22] using the DIM method with high level *ab initio* input diatomic curves. In contrast to the heavier rare gases that exhibit a symmetric triatomic core sharing the charge, the ionic neon clusters have a relatively flexible ionic core with a symmetric tetratomic structure for $n<15$ and asymmetric triatomic structure for $n \geqslant 15$. Extra stability is found for $n=9$ (a ring of 5 atoms around the center of the tetratomic core), 14 (two staggered 5-atom rings around the tetratomic core), 18 and 21. These results are in agreement with the experimental findings.[12,13]

Only a few theoretical studies have been performed on the dynamics of ionized neon clusters in the range of the $Ne^+(^2P)$ ground state ion.[23–25] For vertical ionization, Stampfli[23] found that very small clusters dissociate entirely into single atoms and a positively charged dimer. Larger clusters like Ne_{13}^+ first eject rapid atoms, then thermalize and evaporate further atoms, while for the largest clusters like Ne_{55}^+ rapid ejection of neon atoms becomes less important. Satta and Gianturco[24] have modeled the neon trimer photoionization using time-dependent vibrational self-consistent dynamics and Yurtsever and Gianturco[25] have studied Ne_n^+ dynamics at different energies using a model potential. These studies have only considered the ground adiabatic surface of the ionic clusters. In a recent Letter[26] we have presented an approach that takes into account all the potential energy surfaces involved and their couplings. It was applied to the dissociation dynamics of Ne_3 upon ionization in the gas phase and inside helium nanodroplets. The few other theoretical studies that have been conducted at this level of complexity on the fragmentation of ionized rare gas clusters have been performed on argon clusters. The first one was by Kuntz and Hogreve[27] using a classical path surface-hopping method together with DIM potential energy surfaces. A more recent study of Bastida *et al.*[5,28] used mean field ("hemiquantal") dynamics with DIM potential energy surfaces to study the fragmentation of Ar_n^+ ($n=3-6$). This study gave good agreement with experiment, but the fact that the nuclei evolve on an average surface (mean field dynamics) makes the assignment of the fragmentation channels rather subjective.

In the present study, we simulate the fragmentation of larger size ionized neon clusters, using the same approach as in our earlier work.[26] The molecular dynamics with quantum transitions (MDQT) method of Tully[29–31] is applied in conjunction with realistic potential energy surfaces, and nonadiabatic couplings are taken into account. More specifically, the nuclei are made to evolve classically on one adiabatic potential energy surface at a time, and nonadiabatic transitions are reproduced by hops between surfaces. The potential energy surfaces and nonadiabatic couplings are based on the DIM description. We present here the results of the combined MDQT+DIM approach on isolated Ne_n clusters, with n from 3 to 14. The effect of initial excitation of the neutral clusters is tested. Neutral clusters can be warm either because cooling is not complete in the supersonic expansion where they are formed, or because of energy transfer in collisions with a beam of helium atoms used for size selection. The influence of spin-orbit coupling on the dissociation dynamics is also examined. In addition, we show that the MDQT+DIM method expressed in space fixed coordinates implicitly takes into account the electronic to rotation coupling. This implies that the overall nuclear angular momentum is no longer conserved in the usual version of the MDQT method. We design a method to neglect this coupling and therefore ensure conservation of the overall nuclear angular momentum.

The first part of the paper (Secs. II and III) presents methodological aspects. The relation between the momentum adjustment methods presented in Sec. III and conservation of angular momentum is examined in Sec. IV. Finally, the results of the fragmentation dynamics are presented and discussed in Sec. V.

II. METHOD AND SYSTEM

A. Potential energy surfaces

We have used the same potentials and couplings as in Ref. 26. The multidimensional adiabatic potential energy surfaces V_k and the corresponding eigenstates $\Phi_k(r;\mathbf{R})$ describing the ionic neon cluster are obtained using a DIM model[6,21] with the addition of induced dipole-induced dipole interactions[22,32] using the polarizability of the neon atom from Ref. 33 (0.3956 Å^3). The $3n \times 3n$ DIM matrix is expressed in a basis set of three effective p orbitals per atom for the missing electron. The potential energy curves required as inputs for this matrix are taken from the literature: analytical curve for Ne_2 from Ref. 34 and recent *ab initio* calculations[35] for the four Ne_2^+ potentials. The Ne_2^+ *ab initio* points are fitted by analytical curves of the form

$$V(R) = V_{\text{short}}(R) + [V_{\text{long}}(R) - V_{\text{short}}(R)]T(R). \quad (1)$$

For the $^2\Sigma_u^+$, $^2\Pi_g$, and $^2\Pi_u$ states which present a pronounced well, the short-range interaction $V_{\text{short}}(R)$ is taken as

TABLE I. Parameters in a.u. for the analytic forms of the molecular states of Ne_2^+ [Eqs. (1)–(5)]: all parameters result from fitting the *ab initio* points of Ha *et al.* (Ref. 35) except the physically significant C_4 coefficient which was held fixed at the literature value of Ref. 36.

State	$^2\Sigma_u^+$	$^2\Pi_g$	$^2\Pi_u$	$^2\Sigma_g^+$
A_1	7.3985×10^2	3.3947×10^1	1.0584×10^1	6.7394
α_1	1.34516	1.78637	1.55859	1.33906
B_1	-1.4372×10^{-4}	-1.1926×10^{-4}	-6.8647×10^{-5}	4.6780×10^{-5}
β_1	−7.70302	−9.56229	-1.11524×10^1	-2.06319×10^1
A_2	—	—	—	2.1668
α_2	—	—	—	4.65129×10^{-1}
B_2	—	—	—	-5.5612×10^{-4}
β_2	—	—	—	-3.01568×10^1
D_1	-7.3494×10^2	-1.1102×10^1	−2.8539	—
D_2	1.3020×10^2	2.0088×10^2	1.7729×10^2	—
δ	1.34064	1.44868	1.29260	—
a	1.4557	2.3313	3.5366	5.3226
b	7.7849	7.3137	6.1227	7.4765
C_4 (fixed)	−1.335	−1.335	−1.335	−1.335
C_6	-9.7099×10^1	−5.8778	7.1953	-1.1272×10^2
C_8	0	0	1.7557×10^2	1.1935×10^4

$$V_{\text{short}}(R) = A_1 e^{-\alpha_1 R} + B_1 e^{-\beta_1/R} + \sum_{n=1}^{2} D_n e^{-n\delta R}. \tag{2}$$

For the highest state $^2\Sigma_g^+$ which is repulsive, $V_{\text{short}}(R)$ is taken as

$$V_{\text{short}}(R) = \sum_{n=1}^{2} (A_n e^{-\alpha_n R^n} + B_n e^{-\beta_n/R^n}). \tag{3}$$

In Eq. (1), $V_{\text{long}}(R)$ is the long-range ion-induced dipole interaction

$$V_{\text{long}}(R) = \frac{C_4}{R^4} + \frac{C_6}{R^6} + \frac{C_8}{R^8}. \tag{4}$$

Finally, the switching function

$$T(R) = 0.5[1 + \tanh(a(R-b))] \tag{5}$$

ensures a smooth transition between the short and the long range forms. The use of analytical fits avoids spurious nonadiabatic couplings due to the incertitude on the *ab initio* points. The resulting coefficients are collected in Table I. Note that the physically significant C_4 coefficients have been fixed to a common value taken from the literature.[36] This imposes the same dissociation threshold and asymptotic behavior for the four potential energy curves of Ne_2^+. The standard deviation for the fits including all the *ab initio* points is 8, 15, 1, and 27 cm^{-1} for the $^2\Sigma_u^+$, $^2\Pi_g$, $^2\Pi_u$, and $^2\Sigma_g^+$ states, respectively, which is smaller than typical *ab initio* uncertainties. Diagonalization of the resulting H_{DIM} matrix is performed using standard algorithms and provides the $3n$ adiabatic surfaces and their couplings.

B. Spin-orbit coupling

The spin-orbit coupling is treated using the semiempirical treatment of Cohen and Schneider,[37] as presented in Ref. 32. The only input parameter is the spin-orbit splitting between the $^2P_{3/2}$ and $^2P_{1/2}$ states of Ne^+, which is equal to 780.424 cm^{-1}.[35] Effective spin orbitals (6 per atom) are used instead of effective p orbitals for the DIM Hamiltonian. This produces a block-diagonal matrix with two identical blocks which are coupled by the spin-orbit Hamiltonian. The order of the resulting complex matrix is doubled, thus making a calculation including spin-orbit effects computationally much more expensive.

C. Dynamics

Throughout this paper two types of vectors will be encountered. Vectors of the usual three-dimensional space are denoted by an arrow above the letter (e.g., $\vec{X}$), while vectors in the $3n$-dimensional space of the dynamical variables are written in boldface (e.g., $\boldsymbol{X}$). When necessary, $\vec{X}_\alpha$ will denote the three-dimensional vector associated to atom α extracted from the $3n$-dimensional vector $\boldsymbol{X}$. For instance, $\vec{R}_\alpha$ denotes the position vector of atom α with components $\vec{R}_{\alpha 1}$, $\vec{R}_{\alpha 2}$, $\vec{R}_{\alpha 3}$ equal to components $\boldsymbol{R}_{3\alpha-2}$, $\boldsymbol{R}_{3\alpha-1}$, $\boldsymbol{R}_{3\alpha}$ of the $3n$-dimensional vector $\boldsymbol{R}$ of all the Cartesian coordinates.

The MDQT method of Tully[29–31] is used in this work to describe the fragmentation of ionized neon clusters. Electronic degrees of freedom are treated quantum mechanically by propagating a time-dependent electronic wave function, while nuclear coordinates are treated classically in terms of Cartesian positions and momenta. This makes it easy to increase the number of atoms, while taking into account the coupled potential energy surfaces involved in the dynamics. The nuclei evolve on a single adiabatic potential energy surface V_k according to Hamilton's equations of motion. The time-dependent electronic wave function of the system is expanded in the adiabatic basis set $\Phi_l(r;\boldsymbol{R})$,

TABLE II. Minimum ($E_{\min}$) and zero-point energies (ZPE) of Ne_n, and minimum energies of Ne_n^+ without ($E_{\min}$) and with ($E_{\min}^{SO}$) the spin-orbit interaction. $E_{\min}$ and ZPE for the neutral clusters are given in wave numbers and in units of ϵ, the Ne_2 well depth, and compared to the minimum energies of Hoare and Pal (Ref. 39) and to the ZPE energies of Leitner *et al.* (Ref. 40), respectively (see text). The zero for energies is the completely dissociated cluster, i.e., (n Ne) for neutral clusters and $Ne^+(^2P)+(n-1)Ne$ or $Ne^+(^2P_{3/2})+(n-1)Ne$ in the absence or the presence of spin-orbit interaction for ionic clusters.

	Ne_n						Ne_n^+	
n	$E_{\min}$ (cm^{-1}) (this work)	$E_{\min}$ (ϵ) (this work)	$E_{\min}$ (ϵ) (Ref. 39)	ZPE (cm^{-1}) (this work)	ZPE (ϵ) (this work)	ZPE (ϵ) (Ref. 40)	$E_{\min}$ (eV) (this work)	$E_{\min}^{SO}$ (eV) (this work)
2	−29.365	1.000	1.000	−16.982±0.001	−0.5783	−0.5667	−1.509 320	−1.477 706
3	−88.095	3.000	3.000	−51.351±0.002	−1.749	−1.721	−1.644 773	−1.610 017
4	−176.190	6.000	6.000	−103.436±0.004	−3.522	−3.461	−1.699 886	−1.663 678
5	−266.544	9.077	9.104	−157.783±0.006	−5.373	−5.299	−1.748 249	−1.719 063
6	−369.364	12.578	12.712	−219.790±0.009	−7.485	−7.448	−1.798 750	−1.778 332
7	−480.589	16.366	16.505	−289.89±0.02	−9.872	−9.769	−1.849 081	−1.838 040
8	−575.436	19.596	19.821	−348.59±0.02	−11.87	—	−1.899 271	−1.898 283
9	−698.692	23.793	24.113	−426.57±0.02	−14.53	—	−1.951 001	−1.961 534
10	−821.653	27.981	28.422	−505.35±0.03	−17.21	—	−1.991 733	—
11	−945.046	32.183	32.766	−584.56±0.04	−19.91	—	−2.033 760	—
12	−1092.492	37.204	37.968	−682.25±0.05	−23.23	—	−2.075 568	—
13	−1274.269	43.394	44.327	−802.55±0.06	−27.33	−27.119	−2.118 157	—
14	−1373.292	46.766	47.846	−861.94±0.07	−29.35	—	−2.163 193	—

$$\Psi(r,t)=\sum_{l=1}^{N_s} c_l(t)\Phi_l(r;\boldsymbol{R}), \tag{6}$$

where $\boldsymbol{R}$ and r denote the set of classical Cartesian coordinates, and the electronic coordinates respectively, and N_s stands for the number of electronic states ($N_s=3n$ when neglecting the spin-orbit interaction and $6n$ when including it, n being the number of neon atoms). Its time evolution is obtained by solving the coupled differential equations for the modulus and the phase of the complex-valued expansion coefficients $c_l(t)$ as given in Ref. 26. The nonadiabaticity of the dynamics is taken into account by allowing for hops between the N_s surfaces with a hopping probability given by Tully.[29] The electronic wave function coefficients are not modified upon hopping, but the atomic linear momenta are adjusted in order to ensure total energy conservation. Different schemes for adjusting momenta, tested in this work, are presented in Sec. III. Classically forbidden hops are simply rejected, as advocated in Ref. 38.

D. Initial conditions

Initial conditions are selected in order to reproduce the experimental ones as closely as possible.[26] Because of the low temperature in supersonic experiments, clusters are assumed to be in their ground vibrational state. The classical equivalent condition is obtained as follows. Atoms are moved away from their minimum energy position along randomly selected directions until the total energy of the cluster reaches its zero-point energy (ZPE) given in Table II. Note that the relatively large ZPE of the largest clusters compared to the classical minimum energy of smaller size clusters imposed to move several atoms. Energy is then allowed to thermalize during 22 ps by propagation on the potential energy surface of the neutral cluster.

Ionization is then simulated by a vertical transition to a randomly selected ionic surface with a uniform distribution. This uniform probability of the initial electronic surface for the classical motion is mirrored in the electronic wave function by taking identical $c_l(t=0)=1/\sqrt{N_s}$ coefficients in Eq. (6), thus reproducing a coherent excitation of all the excited states involved. Initial geometries for each of the 100 to 500 (depending on the cluster size) trajectories composing a series are obtained by further propagation on the potential energy surface of the neutral cluster for 0.2 ps. In order to avoid problems related to nonergodicity, a complete new trajectory of the neutral is started for the next series.

The minimum energy positions were obtained using a combination of the genetic algorithm by Carroll[41] and Powell's quadratically convergent method.[42] The corresponding structures and energies are compared in Table II with the results of Hoare and Pal.[39,43] Even though a Lennard-Jones potential is used in the work of Hoare and Pal[39,43] instead of Aziz's potential[34] used in this work, the structures obtained are very similar. The zero-point energies presented in Table II have been obtained using an unbiased diffusion Monte Carlo scheme.[44–46] The implementation for the representation of the source term of the random walk uses a combination of weight and branching resulting in a fixed ensemble size[47] similar to the implementation used in Ref. 48. Ensembles of 2000 walkers have been propagated during at least 8000 blocks of 100 to 400 time steps of 100 a.u. The amount of sampling has been tuned in order to have a reasonable correlation length and sufficient accuracy. The error bars given in Table II have been evaluated using one energy per block.

E. Computational details

The mass of the ^{20}Ne isotope, $m=19.992\,435\,6$ a.m.u., has been used in this study.[49] The nonadiabatic couplings are calculated using the Hellmann-Feynman formula with analytical calculation of the gradients of the DIM Hamiltonian. The gradients of the DIM energies for the classical propaga-

tion are also calculated analytically. The corresponding formulas are collected in Appendix A. Since neutral fragments are usually not detected in the experiments, only the charged fragment is further followed in time after a fragmentation event (minimum interfragment atom-atom distance larger than $R_c=8$ Å), thus reducing the computational cost. The maximum propagation time has been limited to 100 ps, but trajectories are stopped earlier if the resulting charged fragment at a dissociation event is found to be stable. A fragment Ne_p^+ is considered as stable if its total internal energy is below the $Ne_{p-1}^+ + Ne$ dissociation threshold, which is equal to the minimum energy of Ne_{p-1}^+. The minimum energies are gathered in Table II. They are obtained using the same method as for the neutral clusters. The corresponding structures have been found to be very similar to those of Naumkin and Wales,[22,43] the slight differences resulting from the different input curves used in the DIM model. The $Ne_n^+ \rightarrow Ne_{n-1}^+ + Ne$ dissociation energy (including spin-orbit interaction) for $6 \leqslant n \leqslant 9$ is about 60 meV, which is very close to the recent experimental results of Gluch *et al.*[14] for $n=10$ obtained from kinetic energy release measurements using a two-sector field mass spectrometer. When the spin-orbit interaction is neglected, results are extracted from 5000 trajectories for each cluster size $n \leqslant 9$ and 1000 trajectories for $9 < n \leqslant 14$. When it is included, the number of trajectories is 5000 for $n \leqslant 4$ and 1000 for $4 < n \leqslant 9$.

III. NONZERO ELECTRONIC ANGULAR MOMENTUM AND MOMENTUM ADJUSTMENT SCHEMES

A. Coupling of electronic states induced by rotation

The use of a basis set of space-fixed p orbitals implies that the coupling between electronic states due to rotation of the molecular system is explicitly taken into account. For instance, in the case of the Ne_2^+ dimer, it can be easily checked (see Appendix B) that for a rotation by θ about the Y axis in the space-fixed frame $\{X,Y,Z\}$, the coupling between the molecular states Σ_u^+ and $\Pi_{x,u}$ of Ne_2^+ due to rotation is given by

$$\frac{d}{d\theta}|\Sigma_u^+\rangle = |\Pi_{x,u}\rangle, \tag{7a}$$

$$\frac{d}{d\theta}|\Pi_{x,u}\rangle = -|\Sigma_u^+\rangle. \tag{7b}$$

In the MDQT method, this coupling appears in the nonadiabatic coupling vector which is used to calculate the hopping probabilities and, in the most common implementations, to adjust momenta at a hopping event. A systematic analysis of the influence of this coupling on the conservation of the total nuclear angular momentum $\vec{N}$ thus seems pertinent.

B. Different methods for adjusting momenta

The adjustment of momenta upon hopping is still an open question.[50] In order to ensure energy conservation, the potential energy discontinuity at a hopping event needs to be compensated by a modification of the kinetic energy. This adjustment requires to specify a direction $\boldsymbol{u}$ in the $3n$ space along which the momenta are modified,

$$\boldsymbol{p}_{\text{after}} = \boldsymbol{p}_{\text{before}} + \zeta \boldsymbol{u}, \tag{8}$$

where ζ is obtained as a solution of the second degree equation imposing energy conservation. The choice of $\boldsymbol{u}$ is not trivial and probably depends on the strength of the couplings involved in the system. We have found that in systems where the electronic orbital angular momentum is nonzero, like in Ne_n^+, some choices may induce a large variation of the overall nuclear angular momentum $\vec{N}$. At a hopping event, the variation of $\vec{N}$ is given by

$$\Delta\vec{N} = \zeta \sum_{\alpha=1}^{n} \vec{R}_\alpha \times \vec{u}_\alpha. \tag{9}$$

We examine below the most commonly used $\boldsymbol{u}$ directions as well as the new ones proposed in this work.

Nonadiabatic coupling vector $\boldsymbol{d}_{kl}(\boldsymbol{R})$. In the original work of Tully,[29,30] the momentum adjustment is made along the nonadiabatic coupling vector $\boldsymbol{d}_{kl}(\boldsymbol{R}) = \langle \Phi_k(r;\boldsymbol{R}) | \nabla_{\boldsymbol{R}} | \Phi_l(r;\boldsymbol{R}) \rangle$. As presented below, we have found that for systems like Ne_n^+, this choice for $\boldsymbol{u}$ can lead to large variations of $\vec{N}$ due to the rotational-electronic coupling. These variations are especially important when the potential energy difference is large, thus requiring large modifications of the momenta [i.e., ζ is large in Eq. (8)]. It should be noted that this nonconservation of $\vec{N}$ is due to the existence of rotational-electronic coupling explicitely taken into account via the DIM model and the coordinates used for the nuclei ($\vec{N}$ is obviously conserved when using internal coordinates or spherical s orbitals).

Gradient $\boldsymbol{g}_{kl}$. One possible choice for $\boldsymbol{u}$ is the gradient of the difference between the two potential energy surfaces involved in the hop, $\boldsymbol{g}_{kl} = \boldsymbol{\nabla}(V_k - V_l)$.[51–54] Because the potential terms V_k and V_l do not depend on the overall orientation of the system, this choice of $\boldsymbol{u}$ cannot induce a change in $\vec{N}$, i.e., Eq. (9) gives $\Delta\vec{N} = \vec{0}$. From the numerical point of view, this choice implies no extra calculations, since the computationally expensive elements from which the gradient is evaluated are already known.

Hessian h_1. Another possible choice for $\boldsymbol{u}$ is the eigenvector $\boldsymbol{h}_1$ corresponding to the largest eigenvalue of the Hessian matrix of the energy difference $\partial^2(V_k - V_l)/\partial \boldsymbol{R}_i \partial \boldsymbol{R}_j$. This method has been proposed and implemented for a two-state model.[55,56] Some modifications with respect to the original procedure[55] are required for cases with a larger dimensionality and/or cases for which the hopping event occurs at a geometry that does not necessarily correspond to the minimum of $V_k - V_l$. At the minimum geometry of $V_k - V_l$, the eigenvectors of the Hessian matrix correspond to first order either to internal vibrations or to overall nuclear rotation. For configurations that do not correspond to an extremum, overall nuclear rotation and vibrations are no longer separated. The eigenvector $\boldsymbol{h}_1$ corresponding to the largest eigenvalue may contain a non-negligible amount of rotation, therefore inducing a nonzero $\Delta\vec{N}$.

Hessian h_2. We also test another eigenvector $\boldsymbol{h}_2$ of the same Hessian matrix. The vector $\boldsymbol{h}_2$ is defined by two conditions: (i) the corresponding eigenvalue has to be nonzero, and (ii) the change in the nuclear rotational angular momentum, Eq. (9), has to be minimum. (Note that $\boldsymbol{h}_2$ and $\boldsymbol{h}_1$ may be identical.)

The fact that the overall nuclear rotation momentum $\vec{N}$ is not conserved is not in itself a problem of the method: it is expected for systems with nonzero rotational-electronic coupling. Nevertheless, we have observed in the case of Ne_n^+ that the magnitude of variation of $\vec{N}$ depends on the choice of $\boldsymbol{u}$. Also, even though the averaged value of N remains small for all methods, the large variation of N for some of the trajectories implies that a large amount of energy has flown into rotation, which could bias averages for other quantities. Since a quantum calculation including the rotational-electronic coupling is hardly feasible even for Ne_3^+, it is not possible to check which method gives the correct answer. This has motivated us to design a new way to adjust momenta that ensures the conservation of $\vec{N}$ upon hopping by neglecting the rotational-electronic coupling. Comparing the original version of the methods with the ones ensuring $\vec{N}$ conservation provides an opportunity to estimate the importance of this coupling in the dynamics. We use a procedure proposed by Jellinek and Li[57] to separate the rotational and the vibrational components of the atomic velocities in a floppy cluster. This procedure is based on the definition of an instantaneous angular velocity vector $\vec{\omega}$ by considering the instantaneous configuration of the system as rigid. In our case, the procedure is directly applied to $\boldsymbol{u}$ as detailed below. The change in instantaneous angular velocity $\Delta\vec{\omega}$ due to momentum adjustment is deduced from $\Delta\vec{N}=\mathcal{I}\Delta\vec{\omega}$ by using Eq. (9) for $\Delta\vec{N}$

$$\Delta\vec{\omega}=\mathcal{I}^{-1}\zeta\sum_{\alpha=1}^{n}\vec{R}_\alpha\times\vec{u}_\alpha, \tag{10}$$

$\mathcal{I}$ being the instantaneous matrix of inertia. The direction $\boldsymbol{u}_{\mathrm{vib}}$ is then defined by subtracting from $\boldsymbol{u}$ the purely rotational contribution

$$\vec{u}_{\mathrm{rot}\ \alpha}=m\Delta\vec{\omega}\times\vec{R}_\alpha, \tag{11a}$$

$$\vec{u}_{\mathrm{vib}\ \alpha}=\vec{u}_\alpha-\vec{u}_{\mathrm{rot}\ \alpha}. \tag{11b}$$

This scheme can be applied to all the methods presented above.

Hopping probability. In the MDQT algorithm, $\boldsymbol{u}$ is the nonadiabatic coupling vector which is also used to determine the hopping probability. This probability depends on the kinetic coupling term $\dot{\boldsymbol{R}}\cdot\boldsymbol{d}_{kl}$, which can be written as

$$\dot{\boldsymbol{R}}\cdot\boldsymbol{d}_{kl}=(\dot{\boldsymbol{R}}_{\mathrm{rot}}+\dot{\boldsymbol{R}}_{\mathrm{vib}})\cdot((\boldsymbol{d}_{kl})_{\mathrm{vib}}+(\boldsymbol{d}_{kl})_{\mathrm{rot}}). \tag{12}$$

In the $\vec{N}=\vec{0}$ case it is obvious that the hopping probability is nonzero only when $(\boldsymbol{d}_{kl})_{\mathrm{vib}}$ is nonvanishing since $\dot{\boldsymbol{R}}_{\mathrm{rot}}=\boldsymbol{0}$ and $\dot{\boldsymbol{R}}_{\mathrm{vib}}\cdot(\boldsymbol{d}_{kl})_{\mathrm{rot}}=0$ (see Appendix C). However, if $\vec{N}\neq\vec{0}$, $(\boldsymbol{d}_{kl})_{\mathrm{vib}}$ can be zero and the hopping probability be nonzero. For such a hop, a momentum adjustment along the $(\boldsymbol{d}_{kl})_{\mathrm{vib}}$ direction is obviously impossible. We thus only use $\dot{R}\cdot(\boldsymbol{d}_{kl})_{\mathrm{vib}}$ for calculating the hopping probability when using $(\boldsymbol{d}_{kl})_{\mathrm{vib}}$ as the $\boldsymbol{u}$ direction. This amounts to neglecting transitions due to rotational-electronic coupling. For the sake of completeness, this modified hopping probability is also tested for other choices of $\boldsymbol{u}$, namely for $\boldsymbol{u}=\boldsymbol{g}_{kl}$, $(\boldsymbol{h}_1)_{\mathrm{vib}}$ and $(\boldsymbol{h}_2)_{\mathrm{vib}}$.

The different possibilities for $\boldsymbol{u}$ combined with the usual and modified hopping probability lead to eight choices. The results of these choices are presented and discussed in the following section, in the case where spin-orbit interactions are neglected.

When spin-orbit interactions are included, the Hamiltonian matrix is no longer real since it is written in the space-fixed frame. This implies that the eigenvectors, hence the nonadiabatic couplings, are complex. Using $\boldsymbol{d}_{kl}$ as the direction along which to adjust momenta and separating out its rotational part could be straightforward by using the modulus of the components instead of the (complex) components themselves, but the justification for doing this is not obvious. We have decided to adjust momenta along $\boldsymbol{\nabla}(V_k-V_l)$ and use the unmodified hopping probability. This choice was motivated by three reasons: (i) contrary to the eigenvectors of the Hamiltonian matrix used to define $\boldsymbol{d}_{kl}$, $\boldsymbol{\nabla}(V_k-V_l)$ only depends on eigenvalues and is therefore real (and conserves $\vec{N}$); (ii) as shown later, $\boldsymbol{u}=(\boldsymbol{d}_{kl})_{\mathrm{vib}}$ or $\boldsymbol{\nabla}(V_k-V_l)$ give very similar results over the whole range of cluster sizes studied in this work and we can expect the same behavior when the spin-orbit interaction is included; (iii) calculations including spin-orbit interactions are much more expensive, hence were restricted to only one method. Note that due to computational cost, calculations are restricted to $n\leqslant 9$ in this case.

IV. RESULTS ON THE CONSERVATION OF $\vec{N}$

As a comparative test of the eight momentum adjustment methods introduced in Sec. III, the average and maximum values of the total nuclear angular momentum $\vec{N}$ at the end of the fragmentation dynamics of isolated Ne_3^+ are presented in Table III. For each case, the maximum and the average $N=|\vec{N}|$ values are obtained from propagating 5000 trajectories during 100 ps starting from a nonrotating cluster, $\vec{N}=\vec{0}$. Examination of the table shows that the conservation of $\vec{N}$ strongly depends on the momentum adjustment method. Methods A, E, and F for which momentum adjustment is made along $\boldsymbol{d}_{kl}$, $\boldsymbol{h}_1$, and $\boldsymbol{h}_2$, respectively, do not conserve $\vec{N}$ because the rotational parts of these vectors are in general not negligible. The largest N value is one order of magnitude larger for $\boldsymbol{d}_{kl}$ than for $\boldsymbol{h}_1$ or $\boldsymbol{h}_2$. The final N distributions for these three methods are presented in Fig. 1. The distribution obtained with $\boldsymbol{u}=\boldsymbol{d}_{kl}$ is much more peaked around $N=0$ than for $\boldsymbol{h}_1$ and $\boldsymbol{h}_2$ as can be seen from the number of trajectories that give $N=1$. On the other hand, it spans a much wider range of N values than the other two (largest value 162 versus 16.2 from Table III). It seems that the criteria used to define $\boldsymbol{h}_1$ and $\boldsymbol{h}_2$, which select eigenvectors of the Hessian matrix with the smallest amount of rotation (largest eigenvalue for $\boldsymbol{h}_1$ or minimization of $\Delta\vec{N}$ for $\boldsymbol{h}_2$) lead to a similar loss of conservation of $\vec{N}$. The deviation from zero of the

TABLE III. Average and maximum N values after fragmentation of $(Ne_3^+)^*$, using eight different momentum adjustment methods at the hops. These methods are defined in Sec. III B. Each line is the result of propagating 5000 trajectories for 100 ps.

Label	$\boldsymbol{u}$	P_{kl}	$\langle N\rangle$ (a.u.)	$N_{\max}$ (a.u.)
A	$\boldsymbol{d}_{kl}$	$\dot{\boldsymbol{R}}\cdot\boldsymbol{d}_{kl}$	5.65	162
B	$(\boldsymbol{d}_{kl})_{\text{vib}}$	$\dot{\boldsymbol{R}}\cdot(\boldsymbol{d}_{kl})_{\text{vib}}$	2.04×10^{-6}	5.98×10^{-4}
C	$\boldsymbol{g}_{kl}$	$\dot{\boldsymbol{R}}\cdot\boldsymbol{d}_{kl}$	1.93×10^{-6}	6.30×10^{-4}
D	$\boldsymbol{g}_{kl}$	$\dot{\boldsymbol{R}}\cdot(\boldsymbol{d}_{kl})_{\text{vib}}$	1.93×10^{-6}	6.30×10^{-4}
E	$\boldsymbol{h}_1$	$\dot{\boldsymbol{R}}\cdot\boldsymbol{d}_{kl}$	0.833	16.2
F	$\boldsymbol{h}_2$	$\dot{\boldsymbol{R}}\cdot\boldsymbol{d}_{kl}$	0.689	9.53
G	$(\boldsymbol{h}_1)_{\text{vib}}$	$\dot{\boldsymbol{R}}\cdot(\boldsymbol{d}_{kl})_{\text{vib}}$	2.16×10^{-6}	8.66×10^{-4}
H	$(\boldsymbol{h}_2)_{\text{vib}}$	$\dot{\boldsymbol{R}}\cdot(\boldsymbol{d}_{kl})_{\text{vib}}$	7.48×10^{-6}	2.26×10^{-2}

mean $\langle N\rangle$ and the largest $N_{\max}$ values obtained with the B, G, and H methods for which the separation of the rotation has been enforced, are of the order of the one determined with $\boldsymbol{g}_{kl}$ (methods C and D)—despite a slight difference in $N_{\max}$ for the H method. This confirms the efficiency of our procedure for neglecting electronic-rotational couplings. There is no rotational contribution to the hopping probability for $\boldsymbol{u}=\boldsymbol{g}_{kl}$ as can be seen by comparing methods C and D in Table III. This is expected for all the $\vec{N}$ conserving methods when $\vec{N}=\vec{0}$ initially, since Eq. (12) then reduces to its vibrational contribution only, $\dot{\boldsymbol{R}}\cdot\boldsymbol{d}_{kl}=\dot{\boldsymbol{R}}\cdot(\boldsymbol{d}_{kl})_{\text{vib}}$.

From now on, we focus on the N conserving methods, i.e., methods B [where the direction for adjusting momenta $\boldsymbol{u}$ is the vibrational part of the nonadiabatic coupling vector $(\boldsymbol{d}_{kl})_{\text{vib}}$ and the hopping probability P_{kl} is proportional to $\dot{\boldsymbol{R}}\cdot(\boldsymbol{d}_{kl})_{\text{vib}}$], C [$\boldsymbol{u}$ is the gradient of the potential energy difference $\boldsymbol{g}_{kl}=\boldsymbol{\nabla}(V_k-V_l)$ and $P_{kl}\propto\dot{\boldsymbol{R}}\cdot\boldsymbol{d}_{kl}$], and D [$\boldsymbol{u}=\boldsymbol{g}_{kl}$ and $P_{kl}\propto\dot{\boldsymbol{R}}\cdot(\boldsymbol{d}_{kl})_{\text{vib}}$]. We no longer consider the methods where momentum adjustment is based on an eigenvector of the Hessian matrix (E, F, G, and H in Table III) because these methods are rarely used in the literature. They are also more expensive in CPU time than the others, and slightly less accurate in our case since the second derivatives involved in the Hessian matrix are evaluated numerically (whereas $\boldsymbol{d}_{kl}$ and $\boldsymbol{g}_{kl}$ are evaluated analytically). Last but not least, the use of these methods is well justified when hops are localized at the minimum of the potential energy difference, which is usually not the case in the MDQT method.

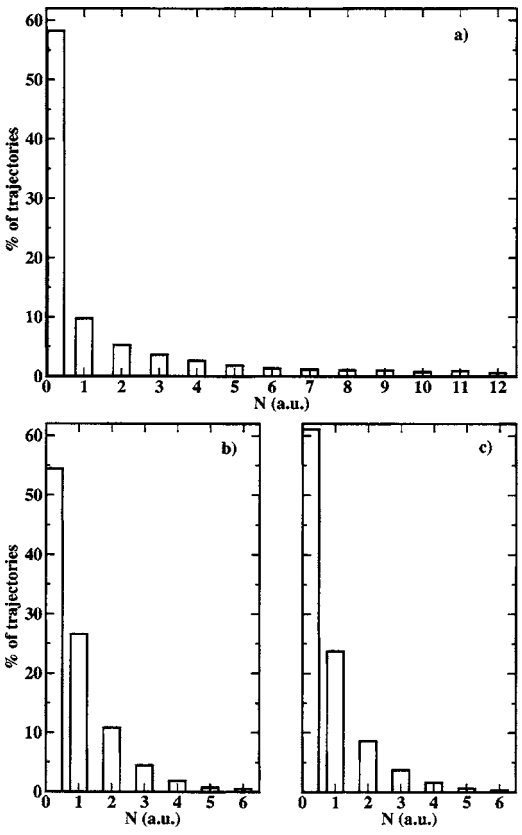

FIG. 1. Final N distribution for 5000 trajectories, using (a) method A ($\boldsymbol{u}=\boldsymbol{d}_{kl}$), (b) method E ($\boldsymbol{u}=\boldsymbol{h}_1$), (c) method F ($\boldsymbol{u}=\boldsymbol{h}_2$), for momentum adjustment at the hops. Note that the range for N has been cut. The maximum N values are given in Table III.

The influence of the three methods (B, C, and D) on the fragmentation pattern of Ne_3 and Ne_4 upon ionization in the gas phase for a temperature around 0 K is presented in Tables IV and V. As discussed above, methods C and D are equivalent in the Ne_3^+ case (see Table IV) since the hopping probability is independent from rotation for $\vec{N}=\vec{0}$. This is no longer the case for Ne_4^+, since Ne_3^+ fragments are produced with $\vec{N}(Ne_3^+)\neq\vec{0}$ after the first fragmentation. The small differences between the C and D methods in Table V confirm that the influence of hops due to rotational-electronic coupling is not very important in the case treated here. Method B also gives results similar to the ones obtained with the other two methods, both for Ne_3^+ (Table IV) and Ne_4^+ (Table V). This shows that the choice of $(\boldsymbol{d}_{kl})_{\text{vib}}$ rather than $\boldsymbol{\nabla}(V_k-V_l)$ as a hopping vector is not critical. In the rest of this work we will focus our attention on the B and C methods.

V. RESULTS OF THE FRAGMENTATION DYNAMICS, $n=3$ to 14

A. Fragmentation patterns

In this section we present and discuss the proportion of final fragments originating from the vertical ionization of Ne_n for $n=3$ to 14. Figure 2 shows the proportion of the three main fragments, Ne^+, Ne_2^+, and Ne_3^+, as a function of the parent size when using the two methods B and C. Figure 2 indicates that Ne_2^+ is the dominant fragment over the whole

TABLE IV. Comparison of methods B, C, and D on the gas phase fragmentation of $(Ne_3^+)^*$ obtained by vertical ionization of Ne_3 clusters. The proportions (in percent) of all the fragmentation channels are reported. They result from propagating a set of 5000 trajectories during 100 ps for each method. No stable Ne_3^+ (A′ or A″) are observed.

Method	$Ne_2^+ + Ne$	$Ne^+ + Ne_2$	$Ne^+ + Ne + Ne$	Time limit reached
B	84.37±0.47	0.62±0.07	14.55±0.41	0.46±0.09
C	84.06±0.36	0.68±0.11	14.78±0.38	0.48±0.10
D	84.06±0.36	0.68±0.11	14.78±0.38	0.48±0.10

range of sizes studied in this work. The amount of fragmentation is quite remarkable: for Ne_{14} which is the largest cluster studied in this work, more than 90% of the clusters give Ne_2^+, 6% give Ne_3^+, and only about 1% have not completed their fragmentation dynamics after 100 ps. The Ne_2^+ proportion rises from 84% for $n=3$ to 99% for $n=8-10$ and then starts to decrease. The complement to 100% mainly comes from Ne^+ fragments for the smaller clusters ($n<9$) and Ne_3^+ fragments for the larger ones ($n>9$). The proportion of Ne^+ decreases from 15% for $n=3$ to 0% for $n=10$. Ne_3^+ fragments only appear for $n \geqslant 7$, and their proportion steadily increases up to 6% for $n=14$ [Fig. 2(c)]. Some stable Ne_4^+ are also formed for the largest clusters ($n=13-14$) but their proportion remains smaller than 0.5%. No noticeable difference in the results is observed when using the B and C methods [respectively, using $(\boldsymbol{d}_{kl})_{\mathrm{vib}}$ and $\boldsymbol{\nabla}(V_k - V_l)$ as hopping vectors], which confirms the conclusion of the preceding section.

The evolution of the fragment proportions as a function of cluster size can be at least partly understood by considering the total energy distributions. As the cluster size increases the total energy is shifted towards negative energies as can be seen from the total energy distributions of $(Ne_3^+)^*$, $(Ne_4^+)^*$, $(Ne_9^+)^*$, and $(Ne_{14}^+)^*$ presented in Fig. 3. This energy decrease favors the formation of Ne_2^+ and Ne_3^+ over Ne^+ which can only be produced when the total energy is positive.

Figure 4 presents the average internal energy per degree of freedom of the parent ions, which can be interpreted as an initial temperature for the ionic clusters. A monotonous decrease with size is observed indicating that $(Ne_n^+)^*$ clusters are cooler when their size increases. This evolution of the parent ions internal energy with increasing size is reflected in the decrease of the Ne_2^+ fragments internal energy presented in Fig. 5. However, the final Ne_2^+ fragment is warmer than the parent ion, indicating that the fragmentation process is far from being evaporative. Let us examine the case of the $(Ne_3^+)^*$ parent as an example: vertical ionization of Ne_3 creates $(Ne_3^+)^*$ with about 0.5 eV of internal energy per degree of freedom (about 1.5 eV in total), while the internal energy of the main resulting fragment Ne_2^+ is 1.2 eV: hence the dissociation of one atom has dissipated about 0.3 eV, but the

TABLE V. Comparison of methods B, C, and D on the gas phase fragmentation of $(Ne_4^+)^*$ obtained by vertical ionization of Ne_4 clusters. Only the proportions of the ionized fragments are reported. They result from propagating a set of 5000 trajectories during 100 ps for each method. No stable Ne_4^+ or Ne_3^+ are obtained.

Method	Stable Ne_2^+	Stable Ne^+	Time limit reached
B	90.10±0.37	9.64±0.30	0.26±0.05
C	88.59±0.32	11.17±0.32	0.24±0.07
D	88.63±0.37	10.85±0.36	0.52±0.11

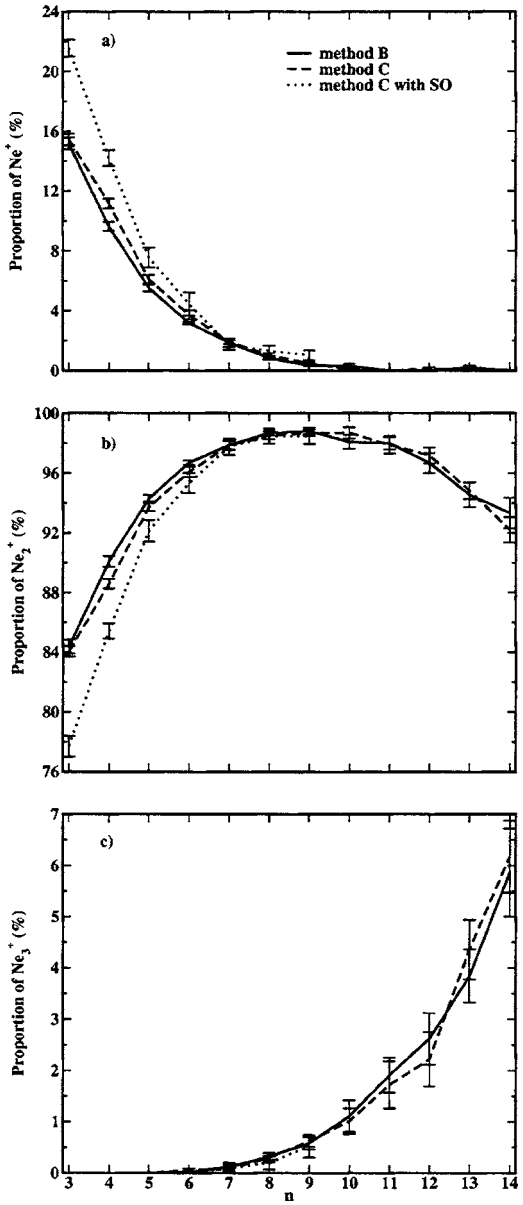

FIG. 2. Proportion of stable (a) Ne^+, (b) Ne_2^+, and (c) Ne_3^+ fragments resulting from the vertical ionization of Ne_n as a function of the initial cluster size ($n=3-14$). Methods B $[\boldsymbol{u}=(\boldsymbol{d}_{kl})_{\mathrm{vib}}]$ and C $[\boldsymbol{u}=\boldsymbol{\nabla}(V_k - V_l)]$ are compared for calculations neglecting the spin-orbit (SO) interaction, while only method C is used when spin-orbit interaction is included. Note that the data in the case with SO are limited to $n \leqslant 9$.

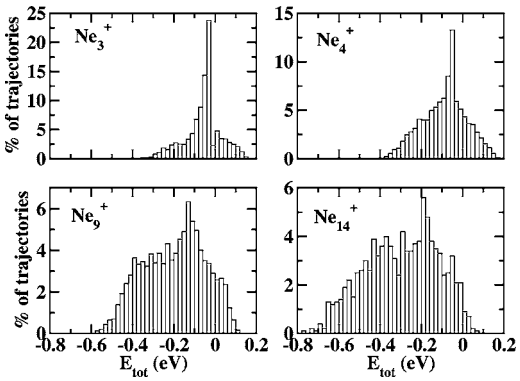

FIG. 3. Comparison of the total energy distribution of the $(Ne_3^+)^*$, $(Ne_4^+)^*$, $(Ne_9^+)^*$, and $(Ne_{14}^+)^*$ clusters without spin-orbit coupling. The energetic interval between two bars is equal to 0.02 eV whatever the cluster size.

internal "temperature" of the cluster has increased rather than decreased. This is true for all the cluster sizes studied here: the internal energy of the main fragment Ne_2^+ is higher than the internal energy per degree of freedom in the parent ion. If the process was evaporative, the warm ionized cluster would cool down by evaporating atoms so that its internal "temperature" would decrease. In the case of the neon clusters studied here, there is too much internal energy deposited in the parent ion for the process to be evaporative, and the internal energy decreases but not the internal "temperature."

We now turn to the effect of spin-orbit interaction on the fragmentation patterns. With the small value of the spin-orbit splitting for Ne^+ (780.424 cm^{-1}), this effect is expected to be small. The fragmentation results are presented in Fig. 2 in comparison with results neglecting this relativistic effect. The proportion of Ne^+ fragments coming from the smaller clusters ($n \leqslant 6$) is clearly increased when spin-orbit interaction is included. The largest effect is observed for the smallest cluster size, $n=3$, for which the proportion of Ne^+ increases to 22% instead of 15%. The difference then gradually disappears and the results for larger clusters ($n \geqslant 6$) are not affected by spin-orbit coupling. This behavior can also be interpreted in terms of energy distributions. Figure 6 displays the total energy distributions of the Ne_n^+ clusters with and without spin-orbit interactions, for $n=3$ and 9. While they are clearly different for Ne_3^+ [Figs. 6(a) and 6(b)], this difference gradually disappears when increasing the cluster size. Indeed, the energy distributions for $n=9$ [Figs. 6(c) and 6(d)]

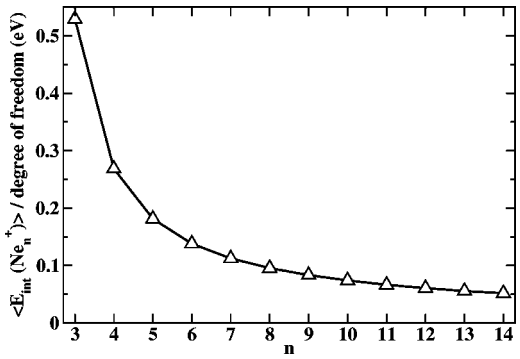

FIG. 4. Average internal energy per degree of freedom of the ionic clusters as a function of the cluster size n.

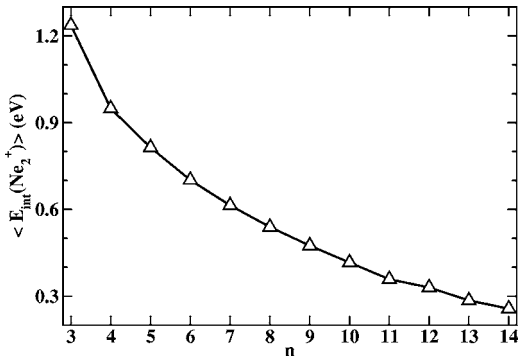

FIG. 5. Mean internal energy of stable Ne_2^+ fragments obtained at the end of the dynamics as a function of the cluster size ($n=3-14$) using the C method.

look quite similar [taking into account the larger noise in Fig. 6(d) due to a smaller number of trajectories]. We infer that the two peaks in Fig. 6(b) are due to the spin-orbit splitting between the $^2P_{1/2}$ and $^2P_{3/2}$ states of Ne^+: since the initial conditions create the ionic cluster in the region of large interatomic distances, they fall close to the asymptotic region where the states separate in two groups connecting to $Ne^+(^2P_{3/2})+2$ Ne and $Ne^+(^2P_{1/2})+2$ Ne. These two groups progressively become scrambled as the cluster size, hence the number of states, increases and the center of the distribution shifts to lower energies. The first consequence of the existence of two peaks for Ne_3^+ is to increase the number of trajectories with a positive energy, hence with the possibility for 3-body dissociation.

B. Fragmentation mechanisms

Figure 7 presents the time-dependent evolution of the intermediate ionic cluster populations during the dissociation of $(Ne_9^+)^*$ clusters, obtained with the C method and without the spin-orbit interaction (similar results are obtained with the B method). As can be seen from the figure, the parent ion population decreases rapidly (after a latency time of about 0.4 ps corresponding to the time necessary for interatomic distances to reach the critical value of 8 Å). During the decrease of the $(Ne_9^+)^*$ population the intermediate Ne_8^+ population raises, then in turn decreases while the population of Ne_7^+ raises and so on, until the main final fragment Ne_2^+ is

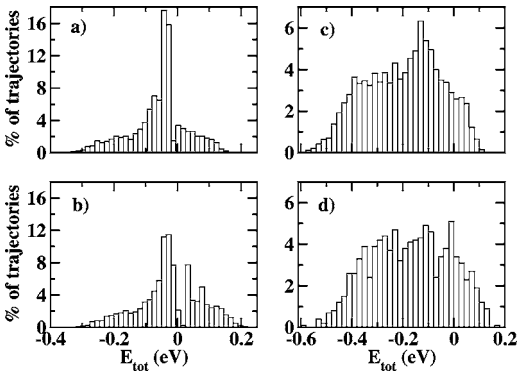

FIG. 6. Comparison of the total energy distribution of the $(Ne_3^+)^*$ and $(Ne_9^+)^*$ clusters with (b) and (d) and without (a) and (c) spin-orbit coupling. The energetic interval between two bars is equal to 0.015 eV for $(Ne_3^+)^*$ and 0.02 eV for $(Ne_9^+)^*$.

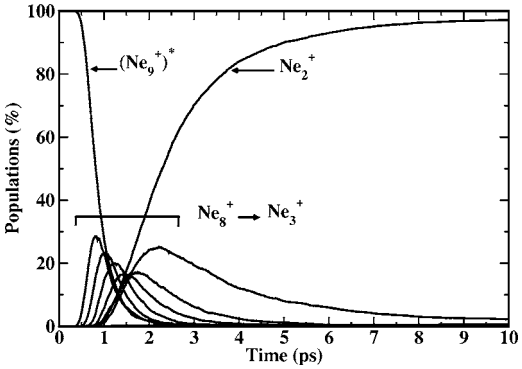

FIG. 7. Time-dependent evolution of the intermediate populations for $(Ne_9^+)^*$ clusters over a set of 5000 trajectories propagated using the C method.

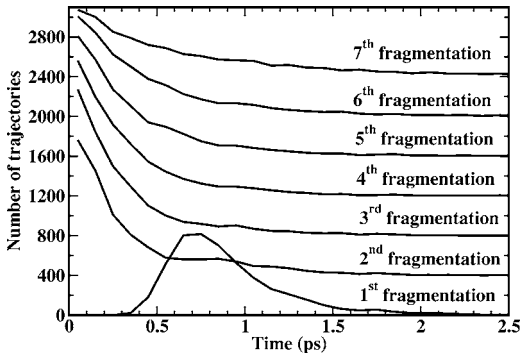

FIG. 9. Time interval between two successive fragmentation events in picoseconds for Ne_9^+. For the sake of clarity, curves have been vertically shifted by $400\times(q-1)$ where q is the evaporation number.

obtained. The whole dynamics is almost over in 10 ps, even though trajectories are run for 100 ps to ensure the convergence of the Ne_3^+ and Ne^+ fragment populations and to minimize the number of trajectories reaching the time limit (about 0.5% or less for $n\leqslant 9$, slowly increasing up to $1.4\pm 0.4\%$ for $n=14$).

The population curves of Fig. 7 seem to indicate that fragmentation is sequential. However, a more detailed inspection reveals that this fragmentation does not generally occur atom by atom. As an example, the excited parent ion $(Ne_9^+)^*$ gives more than 98% of stable Ne_2^+: around 64% of these Ne_2^+ fragments come from Ne_3^+ intermediates, around 15% come from Ne_4^+, etc. and 1% directly come from $(Ne_9^+)^*$ itself. Figure 8 presents a comparison between the average number of fragmentation events in our calculation and the theoretical number of fragmentation events assuming an atom by atom evaporation. This reference curve is obtained by averaging p, the maximum number of fragmentations required to obtain fragment Ne_{n-p}^+, over the final fragment proportions (the resulting curve is very close to $n-2$ since Ne_2^+ is the dominant fragment). The difference between the two curves indicates that several atoms can escape the cluster at the same time. This is more and more true as the cluster size increases: for $n=14$ only eight fragmentation events on average lead to the main fragment Ne_2^+.

Figure 9 presents the distribution of the time interval between two successive fragmentation events for Ne_9^+. Note that a fragmentation event can imply several atoms, which explains why the total number of trajectories decreases with the fragmentation number. Atoms that dissociate within 0.01 ps from each other are counted as belonging to the same event. Except for the first one, all fragmentations exhibit a maximum near zero which reveals a large number of simultaneous atomic departures. This number of simultaneous atomic dissociations decreases with the size of the intermediate cluster, which indicates that the great amount of energy at the beginning of the dynamics is largely responsible for the behavior. The addition of the spin-orbit interaction does not change these fragmentation mechanisms in a significant way.

The decay curve of the $(Ne_n^+)^*$ parent ions can be characterized by their lifetimes (discarding the latency time). They are displayed in Fig. 10 for the cases where spin-orbit interaction is neglected or included. No lifetime has been determined for $(Ne_3^+)^*$ without spin-orbit because of the presence of two uncoupled symmetries (A′ and A″) which have each one their own dynamical decay. The spin-orbit interaction breaks this symmetry rule and a determination of the lifetime is then possible. The lifetime decreases rapidly with the size of the initial cluster for $n\leqslant 5$, and then keeps decreasing but less rapidly. In principle, since the average internal energy per degree of freedom ("temperature") of the initial cluster decreases with size, the lifetime of the parent ion should increase with size. However, several facts go against this argument. First, the initial internal energy is very high and chances are that the initial dissociation steps are not

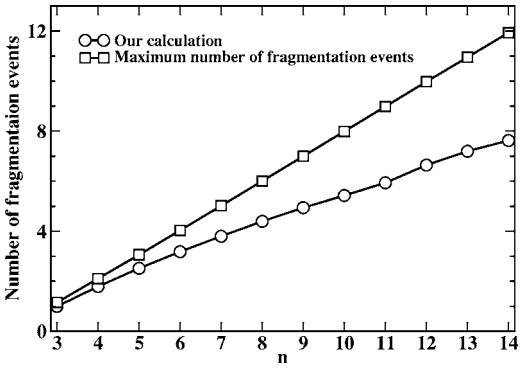

FIG. 8. Average number of fragmentation events as a function of the cluster size ($n=3-14$) (circles) compared with the number of events characterizing an atom by atom evaporation (squares).

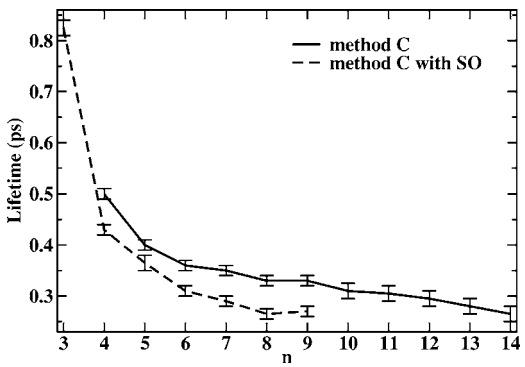

FIG. 10. Decay lifetimes in ps of the $(Ne_n^+)^*$ parent ions as a function of their size, with and without spin-orbit coupling.

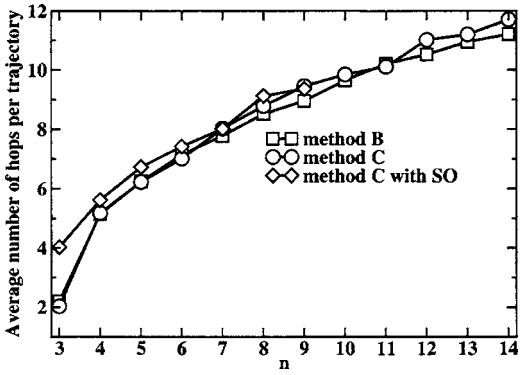

FIG. 11. Mean number of hops during the dynamics as a function of the cluster size (n=3–14).

statistical.[14] Second, the number of coupled electronic states increases with cluster size, hence so does the number of electronic transitions, which makes the relaxation more efficient. The same argument could explain why including the spin-orbit coupling leads to shorter lifetimes, since the number of coupled electronic states is then doubled.

Figure 11 confirms this argument by analyzing the importance of the nonadiabaticity of the dynamics. It represents the mean number of hops during the dynamics as a function of the cluster size. This number is monotonically increasing with cluster size independently of the momentum adjustment method used (B or C methods) and the inclusion or not of spin-orbit interaction. Figure 12 investigates which part of the dynamics is most sensitive to nonadiabaticity. It shows the instants of the mean hops observed in the dynamics of $(Ne_4^+)^*$, $(Ne_6^+)^*$, and $(Ne_9^+)^*$ parent ions. Only hops which occur in at least 1000 trajectories (i.e., 20% of the total number of trajectories) are presented. It is striking to observe that most of the hops occur during the first 1 ps of the dynamics. A larger number of hops at the beginning is expected since the internal energy is higher, hence nonadiabatic couplings are stronger, but the overall time of the whole dissociation process is still about ten times larger. Increasing the cluster size leads to a decrease of the time interval between two successive hops, hence to an acceleration of the nonadiabatic dynamics. For instance at 0.7 ps there have been on average six nonadiabatic transitions for the $(Ne_4^+)^*$ dynamics, nine for

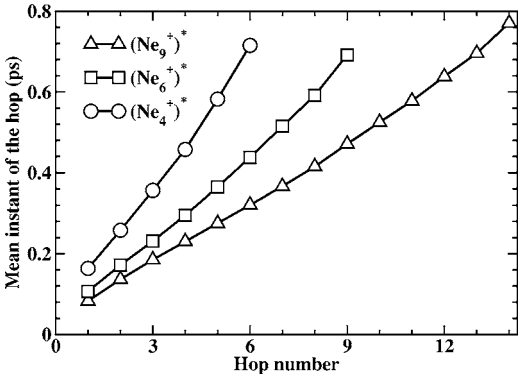

FIG. 12. Mean instant of the first allowed hops for Ne_4^+, Ne_6^+, and Ne_9^+ clusters.

$(Ne_6^+)^*$, and 13 for $(Ne_9^+)^*$. This is directly related to the increasing number of coupled electronic states since internal energy does not increase with size.

C. Effect of an excitation of the neutral clusters

In the experiments in which size selection of the neutrals has been performed,[2] the collision with helium atoms used for size selection warms up the clusters, which can affect their dissociation dynamics. Using the same models as Meyer and Buck,[2] we have estimated a maximum amount of energy transfer of 268 cm^{-1} for n=4 (45 cm^{-1} per degree of freedom), and 320 cm^{-1} for n=9 (15 cm^{-1} per degree of freedom). In order to investigate the influence of internal energy on the dynamics, we have added 10 cm^{-1} per degree of freedom to the Ne_4 and Ne_9 ZPE before studying the fragmentation of the corresponding ion. This amount of internal energy is already large enough that evaporation (vibrational predissociation) of atoms from the neutral cluster becomes an issue, especially for Ne_4: initial conditions which correspond to dissociating neutral clusters are discarded. These calculations have been performed on 5000 trajectories without taking into account spin-orbit couplings. The main fragment is Ne_2^+, the other contribution coming from Ne^+. The proportion of Ne^+ is about 10% and 1% for the $(Ne_4^+)^*$ and $(Ne_9^+)^*$ parent ions, respectively. The corresponding values for the fragmentation of "cold" clusters are 11% and 0.5%. These results suggest that the increase in the initial neutral cluster energy does not influence the final proportions of fragments. This confirms the assumption made by Buck and Meyer[4] for the dissociation of Ar_n^+ after size selection of the neutral clusters by collision with a beam of helium atoms. Bastida *et al.*[5] also found no significant change in the fragment proportions from $(Ar_3^+)^*$ in the range 10 to 25 meV of internal energy.

VI. CONCLUSIONS

We have studied the fragmentation of neon clusters upon ionization, for clusters with 3 to 14 atoms, taking into account all the potential energy surfaces involved and their couplings. Nonadiabatic couplings are shown to be essential, especially at the beginning of the dynamics when the intermediate fragments still have a lot of internal energy. Ne_2^+ is found to be the main fragment with a maximum of 99% for fragmentation after ionization of Ne_9. Ne^+ is the second main fragment for smaller sizes and Ne_3^+ for larger sizes. This behavior can be understood from the initial total energy distribution originating from vertical ionization of the neutral clusters. For smaller sizes this distribution has a relatively important weight at positive energies which allow complete dissociation hence the formation of Ne^+. The distribution shifts to lower, negative energies with increasing size, which favors the formation of larger fragments. The internal energy of the main fragment, Ne_2^+, is also found to decrease with initial cluster size. The preference for the dimer ion as the primary product of larger clusters fragmentation was explained in a model proposed by Haberland,[58] based on an analogy with solid state mechanisms. In this model, ionization creates an $(Rg_2^+)^*$ embedded dimer ion which carries a

large excess of internal energy because of the shifted potential energy minimum of the ion with respect to the neutral (about 1.2 eV for argon). This energy is released to the surrounding cluster by coupling of the vibrational motion of the dimer ion to the modes of the cluster, resulting in major fragmentation. Model calculations[59] on argon clusters using this model have indeed shown this effect, with energy relaxation on a time scale of several hundred picoseconds.

Analysis of the fragmentation shows that the mechanism is not evaporative: it is rather explosive, with several atoms dissociating at the same time. The very small number of long-lived trajectories (>100 ps) indicates that in a typical mass spectrometry experiment, the dissociation dynamics of all the clusters up to $(Ne_{14}^+)^*$ is over by the time the clusters have reached the detection region. Hence the evaporative regime observed for Ne_n^+ $(10 \leqslant n \leqslant 20)$ dissociation in experiments like the one by Gluch *et al.*[14] must correspond to much larger parent ions since their experimental time window is about 20–160 μs. In a femtosecond time-resolved experiment on the photoionization of sodium clusters, Baumert *et al.*[60] have shown that direct fragmentation processes are indeed important at short times rather than statistical unimolecular decay: they observe the ejection of neutral dimers and trimers on time scales of 2.5 and 0.4 ps, respectively, which is the same order of magnitude than the dissociation time scale observed in our results, even though the systems are quite different.

The effect of spin-orbit couplings on the dissociation of these clusters has been investigated. As expected the effect was found to be small, except for the smallest sizes: for Ne_3^+, the final proportion of Ne^+ is about 43% higher when spin-orbit coupling is included. This effect is attributed to a difference in total energy distributions that form a peak around the spin-orbit excited energy of $Ne^+(^2P_{1/2})$, i.e., at a positive energy which favors the formation of Ne^+.

We have designed and tested a procedure to separate out the rotational-electronic coupling in order to check the conservation of the total nuclear angular momentum. This procedure can be used in any surface hopping techniques. The effect of the rotational-electronic coupling was found to be small in the studied systems.

In order to assess the validity of the proposed hopping vector, comparison with quantum calculations would be desirable. Unfortunately, due to computer power, these are limited to the smallest cluster size (neglecting the spin-orbit coupling) for which symmetry consideration greatly reduce the dimensionality of the problem. Work on this comparison is currently underway in our group.

In order to compare with available experimental data, study of heavier rare gas like Ar, is planned. For these heavier atoms, the spin-orbit coupling is expected to have a larger effect than for neon clusters, and will be taken into account.

Finally, the study of fragmentation inside helium nanodroplets, modeled as in Ref. 26 by a friction force is in progress.

ACKNOWLEDGMENTS

The authors would like to thank Marius Lewerenz for fruitful discussions and Ken Janda for strong interest in this work. The Calmip computer center of Toulouse is gratefully acknowledged for a grant of computer time. The authors thank the University of Paul Sabatier, Toulouse, for financial support through an ATUPS grant (D.B.) and an APC grant (A.V. and N.H.).

APPENDIX A: ANALYTICAL GRADIENTS AND NONADIABATIC COUPLING VECTORS

Following the Hellmann-Feynman theorem, the gradients $\nabla_{\vec{R}_\alpha} V_k$ $(k=1,\ldots,3n$ and $\alpha=1,\ldots,n)$ used for classical propagation and for momentum adjustment at hopping events in method C are derived analytically using

$$\nabla_{\vec{R}_\alpha} V_k = \nabla_{\vec{R}_\alpha} \langle \Phi_k | H | \Phi_k \rangle = \langle \Phi_k | \nabla_{\vec{R}_\alpha} H | \Phi_k \rangle \tag{A1}$$

and the $3n$-dimensional nonadiabatic coupling vector $\boldsymbol{d}_{kl}$ between state $|\Phi_k\rangle$ and state $|\Phi_l\rangle$ can be written as

$$\boldsymbol{d}_{kl} = \frac{\langle \Phi_k | \nabla_R H | \Phi_l \rangle}{V_l - V_k} \tag{A2}$$

where V_k and V_l are eigenvalues associated to $|\Phi_k\rangle$ and $|\Phi_l\rangle$, respectively.

APPENDIX B: COUPLING BETWEEN Ne_2^+ ELECTRONIC STATES INDUCED BY ROTATION

The Σ_u^+ and $\Pi_{x,u}$ molecular states of Ne_2^+ can be expressed as a function of the effective p orbitals for the missing electron on atom A and B as

$$|\Sigma_u^+\rangle = \frac{1}{\sqrt{2}}(|p_{z_A}\rangle + |p_{z_B}\rangle), \tag{B1a}$$

$$|\Pi_{x,u}\rangle = \frac{1}{\sqrt{2}}(|p_{x_A}\rangle + |p_{x_B}\rangle), \tag{B1b}$$

where $\{x,y,z\}$ is the molecular frame, z being collinear to the molecular axis. Let us examine the case of planar dynamics, in which the y axis coincides with the Y axis of the space-fixed frame $\{X,Y,Z\}$. In a rotation by θ of the molecular frame about the Y axis, the body-fixed p orbitals can be expressed as a function of the space-fixed p orbitals as

$$|p_z\rangle = \cos\theta\,|p_Z\rangle + \sin\theta\,|p_X\rangle, \tag{B2a}$$

$$|p_x\rangle = -\sin\theta\,|p_Z\rangle + \cos\theta\,|p_X\rangle. \tag{B2b}$$

From Eqs. (B2) it can easily be deduced that

$$\frac{d}{d\theta}|p_z\rangle = |p_x\rangle, \tag{B3a}$$

$$\frac{d}{d\theta}|p_x\rangle = -|p_z\rangle, \tag{B3b}$$

so that the coupling between the molecular states of Ne_2^+ due to rotation is given by Eqs. (7).

APPENDIX C: DEMONSTRATION THAT $\dot{\boldsymbol{R}}_{\mathrm{vib}} \cdot (\boldsymbol{d}_{kl})_{\mathrm{rot}} = 0$

The nonzero rotational part of the nonadiabatic coupling vector could *a priori* involve a term of the form $\dot{\boldsymbol{R}}_{\mathrm{vib}} \cdot (\boldsymbol{d}_{kl})_{\mathrm{rot}}$. We show here that this term is actually zero. $\dot{\vec{R}}_{\mathrm{vib}\alpha}$ in Eq. (12) is defined as

$$\dot{\vec{R}}_{\mathrm{vib}\ \alpha} = \dot{\vec{R}}_{\alpha} - \dot{\vec{R}}_{\mathrm{rot}\ \alpha}, \tag{C1}$$

where, following Jellinek and Li,[57] the rotational part of the velocity

$$\dot{\vec{R}}_{\mathrm{rot}\ \alpha} = \vec{\omega} \times \vec{R}_{\alpha} \tag{C2}$$

is the velocity of $\dot{\boldsymbol{R}}_{\alpha}$ if at instant t the cluster were a rigid body rotating with angular velocity $\vec{\omega}$ defined by

$$\vec{N} = \mathcal{I}\vec{\omega}. \tag{C3}$$

By definition,

$$\vec{N} = \sum_{\alpha} m\vec{R}_{\alpha} \times \dot{\vec{R}}_{\alpha} = \sum_{\alpha} m\vec{R}_{\alpha} \times \dot{\vec{R}}_{\mathrm{vib}\ \alpha} + \sum_{\alpha} m\vec{R}_{\alpha} \times \dot{\vec{R}}_{\mathrm{rot}\ \alpha}. \tag{C4}$$

On the other hand, from the definition of $\dot{\vec{R}}_{\mathrm{rot}\ \alpha}$, $\vec{N}$ is also the angular momentum of the instantaneous rigid body:

$$\vec{N} = \sum_{\alpha} m\vec{R}_{\alpha} \times \dot{\vec{R}}_{\mathrm{rot}\ \alpha}, \tag{C5}$$

which implies that

$$\sum_{\alpha} m\vec{R}_{\alpha} \times \dot{\vec{R}}_{\mathrm{vib}\ \alpha} = \vec{0}. \tag{C6}$$

Using Eq. (11), we can write

$$\begin{aligned} \dot{\boldsymbol{R}}_{\mathrm{vib}} \cdot (\boldsymbol{d}_{kl})_{\mathrm{rot}} &= m \sum_{\alpha=1}^{n} \dot{\vec{R}}_{\mathrm{vib}\ \alpha} \cdot (\Delta\vec{\omega} \times \vec{R}_{\alpha}) \\ &= m \sum_{\alpha=1}^{n} (\vec{R}_{\alpha} \times \dot{\vec{R}}_{\mathrm{vib}\ \alpha}) \cdot \Delta\vec{\omega}. \end{aligned} \tag{C7}$$

This is zero from Eq. (C6).

[1] H. Haberland, Surf. Sci. **156**, 305 (1985).
[2] U. Buck, J. Phys. Chem. **92**, 1023 (1988).
[3] P. Lohbrandt, R. Galonska, H. Kim, M. Schmidt, C. Lauenstein, and U. Buck, *Atomic and Molecular Beams—The State of the Art 2000* (R. Campargue, Springer Verlag, Berlin, 2000).
[4] U. Buck and H. Meyer, J. Chem. Phys. **84**, 4854 (1986).
[5] A. Bastida, N. Halberstadt, J. A. Beswick, F. X. Gadéa, U. Buck, R. Galonska, and C. Lauenstein, Chem. Phys. Lett. **249**, 1 (1996).
[6] P. J. Kuntz and J. Valldorf, Z. Phys. D: At., Mol. Clusters **8**, 195 (1988).
[7] T. Ikegami, T. Kondow, and S. Iwata, J. Chem. Phys. **98**, 3038 (1993).
[8] B. Callicoatt, PhD thesis, University of California, Irvine, 1998.
[9] B. E. Callicoatt, K. Förde, T. Ruchti, L. Jung, K. C. Janda, and N. Halberstadt, J. Chem. Phys. **108**, 9371 (1998).
[10] T. Ruchti, K. Förde, B. E. Callicoatt, H. Ludwigs, and K. C. Janda, J. Chem. Phys. **109**, 10679 (1998).
[11] T. Ruchti, B. E. Callicoat, and K. C. Janda, Phys. Chem. Chem. Phys. **2**, 4075 (2000).
[12] T. D. Märk and P. Scheier, Chem. Phys. Lett. **137**, 245 (1987).
[13] M. Fieber, G. Bröker, and A. Ding, Z. Phys. D: At., Mol. Clusters **20**, 21 (1991).
[14] K. Gluch, S. Matt-Leubner, L. Michalak, O. Echt, A. Stamatovic, P. Scheier, and T. Märk, J. Chem. Phys. **120**, 2686 (2004).
[15] C. Klots, J. Phys. Chem. **92**, 5864 (1988).
[16] P. Scheier and T. D. Märk, J. Chem. Phys. **87**, 5238 (1987).
[17] M. J. DeLuca, D. M. Cyr, W. A. Chupka, and M. A. Johnson, J. Chem. Phys. **92**, 7349 (1990).
[18] W. R. Wadt, Appl. Phys. Lett. **38**, 1030 (1981).
[19] F. Y. Naumkin, P. J. Knowles, and J. N. Murell, Chem. Phys. **193**, 27 (1995).
[20] M. Fieber, A. M. G. Ding, and P. J. Kuntz, Z. Phys. D: At., Mol. Clusters **23**, 171 (1992).
[21] F. O. Ellison, J. Am. Chem. Soc. **85**, 3540 (1963).
[22] F. Y. Naumkin and D. J. Wales, Mol. Phys. **93**, 633 (1998).
[23] P. Stampfli, Z. Phys. D: At., Mol. Clusters **40**, 345 (1997).
[24] M. Satta and F. A. Gianturco, Mol. Phys. **100**, 3699 (2002).
[25] E. Yurtsever and F. A. Gianturco, Comput. Mater. Sci., special issue TAMC4 Conference Proceedings (to be published).
[26] D. Bonhommeau, A. Viel, and N. Halberstadt, J. Chem. Phys. **120**, 11359 (2004).
[27] P. J. Kuntz and J. J. Hogreve, J. Chem. Phys. **95**, 156 (1991).
[28] A. Bastida, N. Halberstadt, J. A. Beswick, and F. X. Gadéa, J. Chem. Phys. **104**, 6907 (1996).
[29] J. C. Tully, J. Chem. Phys. **93**, 1061 (1990).
[30] J. C. Tully, Int. J. Quantum Chem. **25**, 299 (1991).
[31] S. Hammes-Schiffer and J. C. Tully, J. Chem. Phys. **101**, 4657 (1994).
[32] M. Amarouche, G. Durand, and J. P. Malrieu, J. Chem. Phys. **88**, 1010 (1988).
[33] H. Hogreve, Chem. Phys. Lett. **215**, 72 (1993).
[34] R. A. Aziz and M. J. Slaman, Chem. Phys. **130**, 187 (1989).
[35] T. H. Ha, P. Rupper, A. Wüest, and F. Merkt, Mol. Phys. **101**, 827 (2003).
[36] A. Carrington, D. I. Gammie, J. C. Page, A. M. Shaw, and J. M. Hutson, J. Chem. Phys. **116**, 3662 (2001).
[37] J. S. Cohen and B. Schneider, J. Chem. Phys. **61**, 3230 (1974).
[38] U. Müller and G. Stock, J. Chem. Phys. **107**, 6230 (1997).
[39] M. R. Hoare and P. Pal, Ann. Phys. (N.Y.) **20**, 161 (1971).
[40] D. M. Leitner, J. D. Doll, and R. M. Whitnell, J. Chem. Phys. **94**, 6644 (1991).
[41] D. L. Carroll, FORTRAN *Genetic Algorithm Driver*, see http://cuaerospace.com/carroll/ga.html
[42] W. H. Press, B. P. Flannery, S. A. Teukolsky, and W. T. Vetterling, *Numerical Recipes in FORTRAN: The Art of Scientific Computing* (Cambridge University Press, Cambridge, 1986–1992).
[43] *Cambridge Cluster Database*, see http://www-wales.ch.cam.ac.uk/wales/ccd
[44] M. A. Suhm and R. O. Watts, Phys. Rep. **204**, 293 (1991).
[45] C. J. Umrigar, M. P. Nightingale, and K. J. Runge, J. Chem. Phys. **99**, 2865 (1993).
[46] B. L. Hammond, W. A. Lester, and P. J. Reynolds, *Monte Carlo Methods in Ab Initio Quantum Chemistry* (World Scientific, Singapore, 1994).
[47] M. Lewerenz (private communication).
[48] D. Blume, M. Lewerenz, F. Huisken, and M. Kaloudis, J. Chem. Phys. **105**, 8666 (1996).
[49] I. Mills, T. Cvitas, K. Homann, N. Kallay, and K. Kuchitsu, *Quantities, Units and Symbols in Physical Chemistry* (Blackwell Scientific, Oxford, UK, 1988).
[50] C. W. Eaker, J. Chem. Phys. **87**, 4532 (1987).
[51] N. C. Blais and D. G. Truhlar, J. Chem. Phys. **79**, 1334 (1983).
[52] N. C. Blais, D. G. Truhlar, and C. A. Mead, J. Chem. Phys. **89**, 6204 (1988).
[53] M. S. Topaler, T. C. Allison, D. W. Schwenke, and D. G. Truhlar, J. Phys. Chem. A **102**, 1666 (1998).
[54] M. D. Hack, A. W. Jasper, Y. L. Volobuev, D. W. Schwenke, and D. G. Truhlar, J. Phys. Chem. A **103**, 6309 (1999).
[55] J. R. Stine and J. T. Muckerman, J. Chem. Phys. **65**, 3975 (1976).
[56] C. A. Mead and D. G. Truhlar, J. Chem. Phys. **84**, 1055 (1986).
[57] J. Jellinek and D. H. Li, Phys. Rev. Lett. **62**, 241 (1989).
[58] H. Haberland, in *Electronic and Atomic Collisions* edited by J. Eichler, L. V. Hertel, and N. Stolterfoht, (North Holland, Amsterdam, 1983).
[59] J. M. Soler, J. J. Sáenz, N. García, and O. Echt, Chem. Phys. Lett. **109**, 71 (1984).
[60] T. Baumert, C. Röttgermann, C. Rothenfusser, R. Thalweisser, V. Weiss, and G. Gerber, Phys. Rev. Lett. **69**, 1512 (1992).